Impulse Vector Characteristics of a Laser Ablation Propulsion System

IEPC-2013-181

Presented at the 33rd International Electric Propulsion Conference,
The George Washington University • Washington, D.C. • USA
October 6 – 10, 2013

Takumi Oyama[1]
Tokai University, Hiratsuka, Kanagawa, 259-1292,Japan

Hideyuki Horisawa[2]
and

Yuji Oigawa[3] and Keiji Hagiwara[3]

Abstract: In this study, direct focusing of repetitive high-power laser pulses on an arbitrary surface of the vehicle in atmosphere were proposed, in which a blast wave was generated at each pulse and pushes the vehicle on the surface inducing an impulse or thrust vector. A fundamental investigation was conducted on interaction of a focused high-power laser pulse, or blast wave, and the surface with arbitrary shape. Numerical simulation on characteristics of impulse, or thrust, vector generation on the surface was conducted. As the first step of the simulation, for simplicity, some fundamental shapes of the surface, or a vehicle, were assumed, which were planar and semicircular bodies, and shock-surface interactions were investigated. In addition, an experimental investigation on impulse vector characteristics was also performed. From these results, it was shown that a composition of the impulse vector (or each component) reached about 90% of total impulse at initial 10 μsec. In addition, it was also shown that during this duration, a significantly high-pressure region, induced by the shockwave, acting on the surface vectors, which induces a primary thrust, was localized at near laser-irradiation spot. From these results, it was concluded that the directions of impulse vectors were primarily determined by the direction of local surface vectors of laser-irradiation spots.

Nomenclature

r	=	Model radius
θ	=	Angle of laser irradiation spot
α	=	Nozzle angle
t	=	Time

I. Introduction

Kantrowitz introduced the concept of propelling a vehicle by absorbing laser irradiation from a remotely stationed high-power laser [1,2]. In an atmosphere, the physics of the initial interaction between a high-power laser beam and a surface is strongly influenced by the presence of air above the surface. Before a jet of absorbing vapor can be obtained, the air above the surface may break down, and a laser-supported detonation wave will be initiated [3,4]. Air breakdown then occurs in the focal region of the parabola[5]. As for the nozzle shapes, Ageev et al. studied the influence of nozzle geometry on impulse generation using conical and parabolic nozzles and found an optimum nozzle length for certain laser pulse energy [6]. Myrabo et al. found optimum laser pulse energy for a certain nozzle geometry [7]. Mori et al. studied the aerodynamic

[1] Under graduate student, Department of Aeronautics and Astronautics , twist21tkm@gmail.com
[2] I Professor, Department of Aeronautics and Astronautics
[3] Graduate student, Department of Aeronautics and Astronautics

transformation from the blast wave to the impulsive thrust in a nozzle to have a general scaling law [8]. After Myrabo et al.'s first successful flight experiments, similar investigations were reported from other countries including vertical free flights and horizontal wire-guided flights [9].

In this study, unlike the above previous studies, authors propose direct focusing of repetitive high-power laser pulses on an arbitrary surface of the vehicle in atmosphere, in which a blast wave is generated at each pulse and propels the vehicle on the surface inducing an impulse or thrust vector. A fundamental investigation was conducted on interaction of a focused high-power laser pulse, or blast wave, and the surface with arbitrary shape. Numerical simulation on characteristics of impulse, or thrust, vector generation on the surface was conducted. As the first step of the simulation, for simplicity, some fundamental 2-dimensional shapes of the surface, or a vehicle, were assumed and tested, which were planar and semicircular bodies.

II. Computational Method

In our numerical simulation, a commercial computational fluid dynamics (CFD) code, CFD++ (Metacomp Technologies) was utilized. This code solves unsteady compressible Navier-Storkes equations using Total Variation Diminishing (TVD) discretization scheme. An MUSCL scheme with second order interpolation was employed for higher spatial accuracies. An Euler implicit method was also employed for time integration. For evaluation of flow flux, an HLLC method was used.

In this study, a fundamental investigation was conducted on direct focusing of repetitive high-power laser pulses on an arbitrary surface of the vehicle in atmosphere, in which a blast wave is generated at each pulse and pushes the vehicle on the surface inducing an impulse or thrust vector. Numerical simulation was conducted on interaction of a focused high-power laser pulse, or blast wave, and the surface with arbitrary shape. As the first step of the simulation, for simplicity, some fundamental 2-dimensional shapes of the surface, or a vehicle, were assumed and tested. A schematic of the vehicle is shown is Fig.1 where definition of radius r and nozzle angle α is schematically illustrated. The parameters of the models are listed in the table 1. In addition the schematic diagram of the nozzle angle and various laser irradiation spots were tested with angles of θ = 90 deg (center), 60 deg and 30 deg for Model-1 as shown schematically in Fig.2. For Model-2, the angles were θ = 90 deg (center), 75 deg and 60 deg. For Model-P, the angles were θ = 90 deg (center), 76 deg and 66 deg. A horizontal (x-axis) and vertical (y-axis) components of the thrusts, or impulses, induced with the motion of a shock wave, were evaluated to predict the motion of the vehicle.

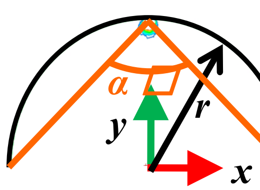

Figure 1 schematic of the analysis model.

Table 1 Model parameters

Model number	Model-1	Model-2	Model-P
Nozzle angle, α: deg	90	135	180
Radius, r: mm	25	25	25 (half width)

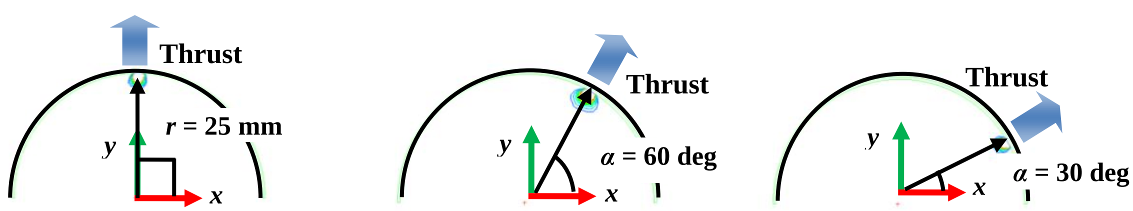

(a) θ = 90 deg **(b) θ = 60 deg** **(c) θ = 30deg**

Figure 2 Schematics of laser irradiation and thrust vector generation in Model-1.

An initial blast wave with circular shape was assumed to be a point explosion model having a radius of 1 mm (with width of 25 mm), a pressure of 8,000 MPa, and a temperature of 5,000 K.

III. Computational Results

A. Histories of Thrust and Pressure Contours (Model-1)

Example of typical temporal thrust variations are shown in Fig.3 (a) and (b), where the instantaneous thrusts are obtained with the integration of local pressures multiplied by surface vectors of the local elements throughout the

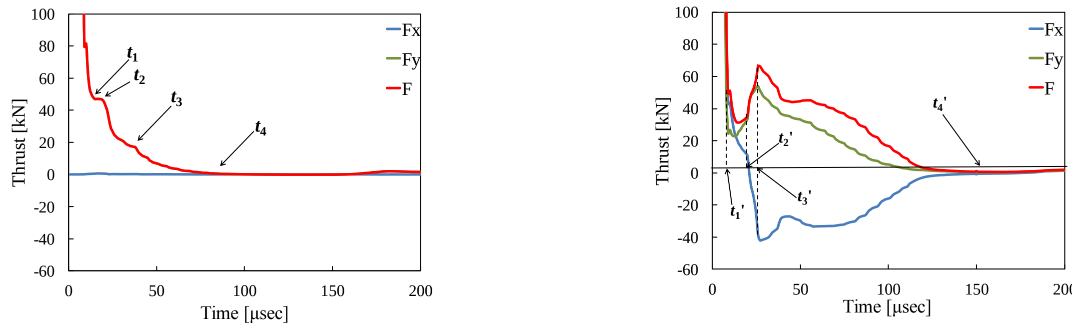

(a) θ = 90 deg **(b) θ = 60 deg**

Figure 3 Example of typical temporal thrust variations.

upper and lower surfaces. For convenience, typical events for θ = 90 deg were denoted as follows; t_0: laser irradiation, t_1: when *y*-component thrust reaching the minimum value, t_2: when *y*-component thrust reaching the second peak, t_3: when a shock wave front reaching a target edge, and t_4: when a total thrust converging zero. On the other hand, for different αs, those events were different and denoted as follows; t_0': laser irradiation, t_1': when a shock wave reaching an edge of the target, t_2': when *x*-component thrust crossing zero, t_3': when *x*-component thrust reaching the minimum value and *y*-component thrust reaching the second peak value, and t_4': when thrust converging zero.

Fig.4 to 9, respectively, show the thrust history and corresponding pressure contours using Model-1 in the case of α = 90 deg, α = 60 deg, α = 30 deg.

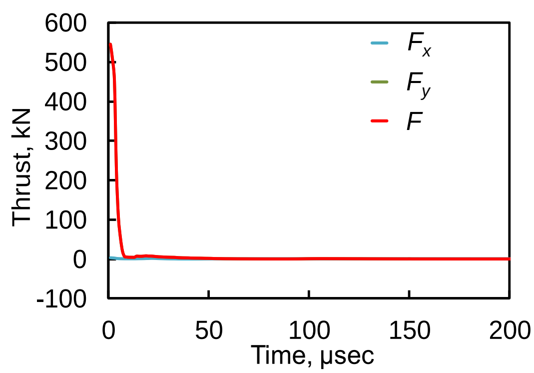

Figure 4 Thrust history, *Model-1 α = 90 deg , θ = 90 deg*

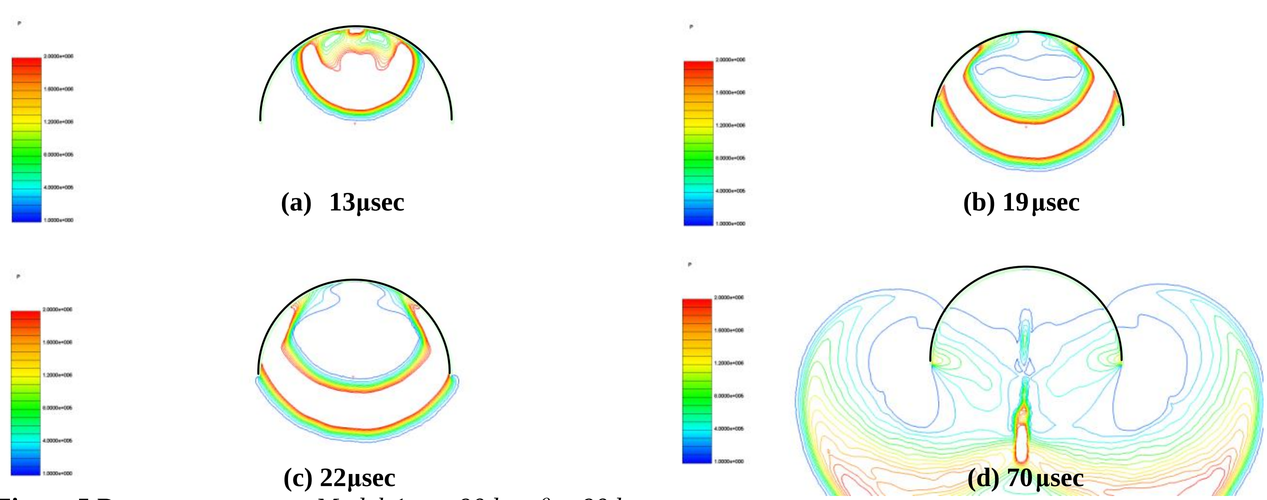

(a) 13μsec **(b) 19μsec**

(c) 22μsec **(d) 70μsec**

Figure 5 Pressure contours, *Model-1 α = 90deg, θ = 90deg*

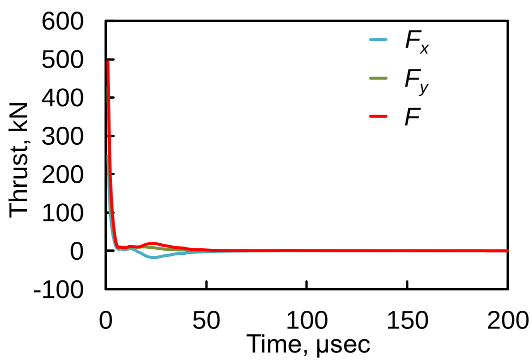

Figure 6 Thrust history, *Model-1 α = 90 deg, θ =60 deg*

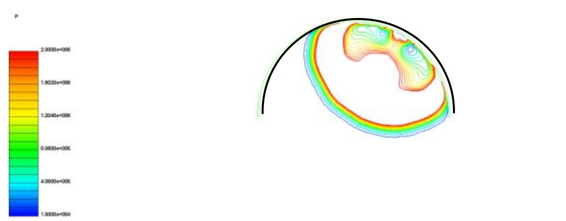

(a) 11 μsec

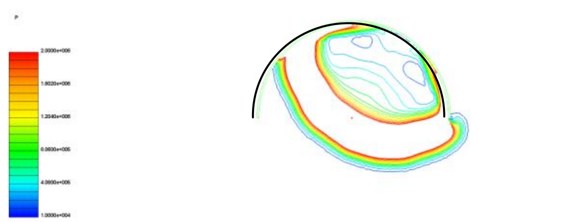

(b) 15 μsec

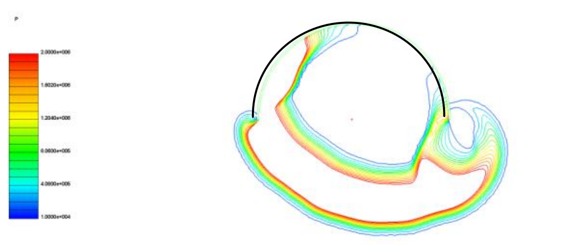

(c) 24 μsec

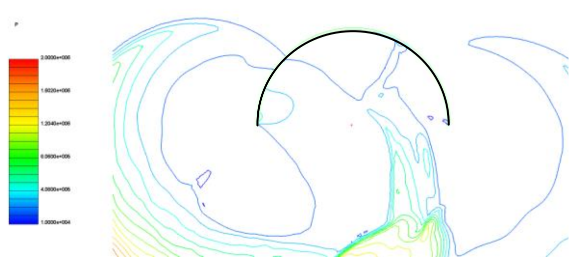

(d) 74 μsec

Figure 7 Pressure contours. *Model-1 α = 90 deg , θ =60 deg.*

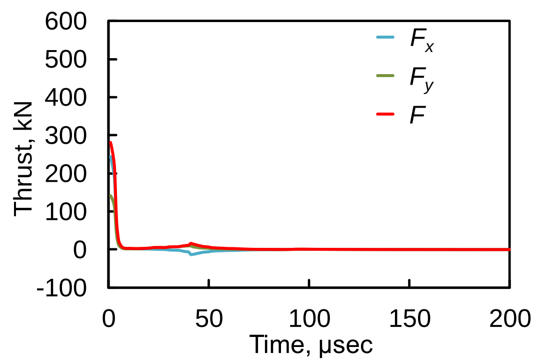

Figure 8 Thrust history. *Model-1 α = 90 deg, θ =30 deg.*

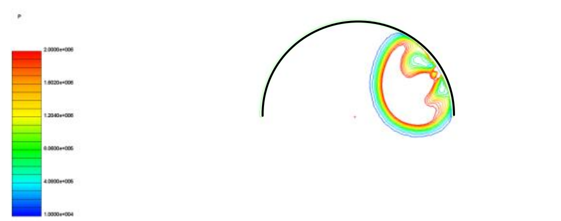

(a) 10 μsec

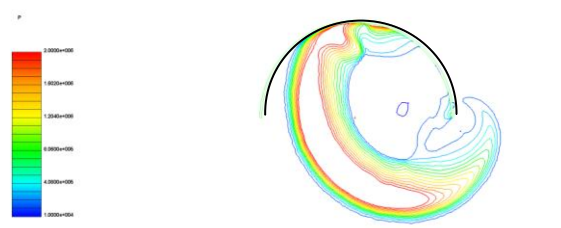

(b) 28 μsec

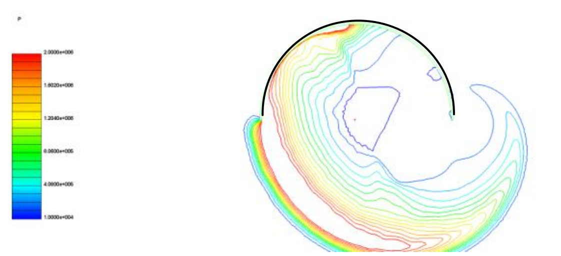

(c) 41 μsec

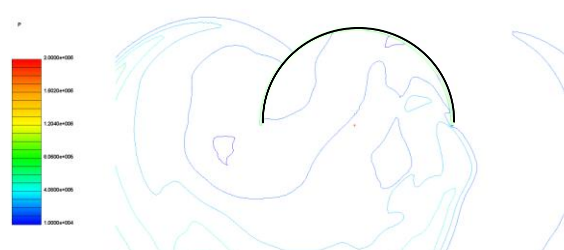

(d) 88 μsec

Figure 9 Pressure contours. *Model-1 α = 90 deg, θ =30 deg.*

On the other hand, y-component thrust reaches the second peak (see Fig. 9(c), t_3'). When a shock wave turns around the edge, a large pressure starts acting on an upper side of the target. Due to this pressure, a negative thrust is induced, and then the x-component becomes negative. After t = 41 μs, x- and y-component thrusts converges into zero (see Fig. 9(d), t_4').

From Fig.4, 6 and 8, it is shown that a composition of the impulse vector (or each component) reaches about 90% of total impulse at initial 10 μsec. From Figs.5, 7, and 9, it is shown that during this duration, a significantly high-pressure region, induced by the shockwave, acting on the surface vectors, which induces a primary thrust, is localized at near laser-irradiation spot.

B. Histories of Thrust and Pressure Contours (Model-2)

Fig.10-15, respectively, show the thrust history and corresponding pressure contours using Model-2 in the case of α = 90 deg, α = 75 deg, α = 60 deg.

Fig. 10 and 11, respectively, show the thrust history and corresponding pressure contours using Model-2 for θ = 90 deg. In Fig. 10, for θ = 90 deg, an explosion starts at t = 0 μs. An initial y-component thrust is about 600 kN. Although, x-component thrusts stay almost zero values, small non-zero values of the x-component thrusts appear due to some asymmetric phenomena. However, shown in the nest section, a total x-component impulse is zero in this case.

At t = 6 μs, a y-component thrust reaches the minimum value (see Fig. 11(a), t_1), and then the thrust slightly increases at t = 10 μs (see Fig. 11(b), t_2). A shock wave reaches the target edge at t = 12 μs (see Fig. 11(c), t_3). After t = 12 μs, the heated air starts to be exhausted and thrust decreases gradually. At t = 65 μs thrust becomes zero (see Fig. 11(d), t_4).

Fig. 12 and 13, respectively, show the thrust history and corresponding pressure contours using Model-2 for θ = 75 deg. In Fig. 11, for θ = 75 deg, an explosion starts at t = 0 μs. Initial y- and x- component thrusts are about 500 kN and 100 kN, respectively. A shock wave reaches the target edge at t = 10 μs (see Fig. 13(a), t_1'). At t =14 μs, x-component thrust becomes zero (see Fig. 13(b), t_2'). Moreover, it reaches the minimum (negative) value at t = 25 μs (see Fig. 13(c), t_3'). After t = 25 μs, oscillating to positive and negative, the x-component thrust gradually balances. At t = 88 μs, both x- and y- components converge into zero (see Fig. 13(d), t_4').

Fig. 14 and 15, respectively, show the thrust history and corresponding pressure contours using Model-2 for θ = 60 deg. In Fig. 14, for θ = 60 deg, an explosion starts at t = 0 μs. Initial y- and x-component thrusts are about 400 kN and 200 kN, respectively. A shock wave reaches the target edge at t = 7 μs (see Fig. 15(a), t_1'). At t = 14 μs, x-component thrust crosses zero, and y-component thrust increases (see Fig. 15(b), t_2'). At t = 26 μs, x-component thrust reaches the minimum value. On the other hand, y-component thrust reaches the second peak (see Fig. 15(c), t_3'). After t = 26 μs,

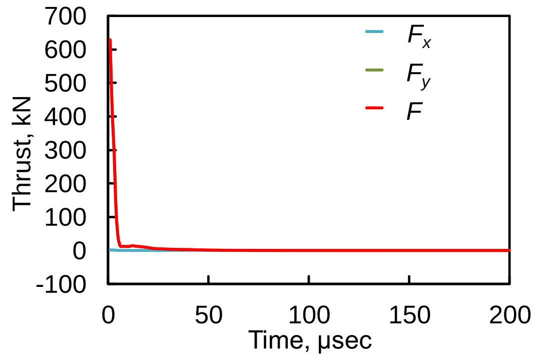

Figure 10 Thrust history. *Model-2 α = 135 deg, θ=90 deg.*

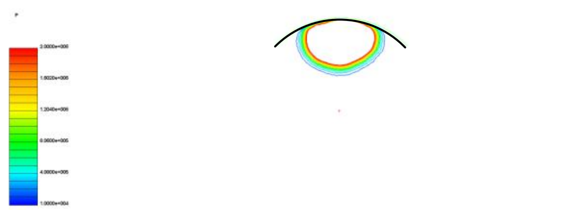

(a) 6 μsec

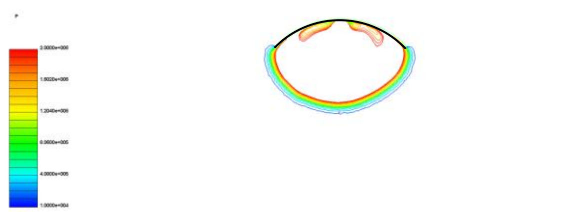

(b) 10 sec

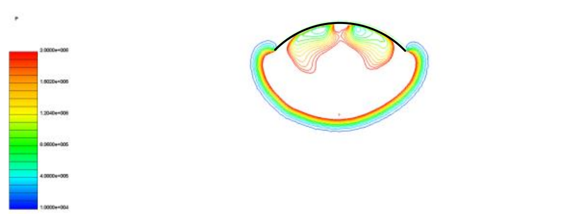

(c) 12 μsec

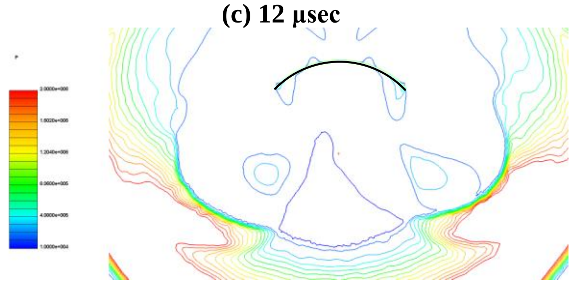

(d) 65 μsec

Figure 11 Pressure contours. *Model-2 α = 135 deg, θ=90 deg.*

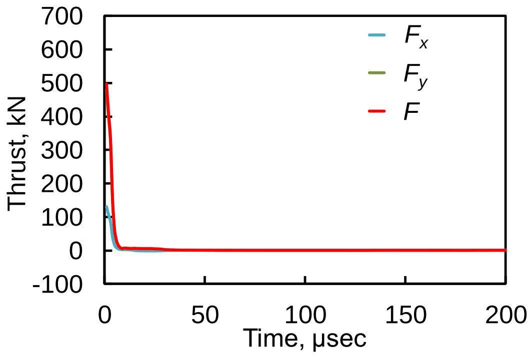

Figure 12 Thrust history. *Model-2 α = 135 deg, θ =75 deg.*

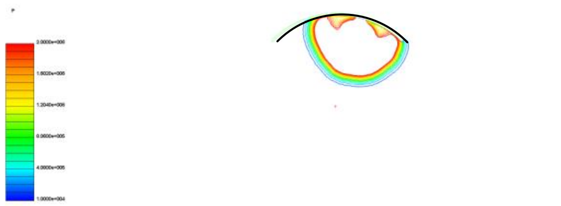

(a) 10 μsec

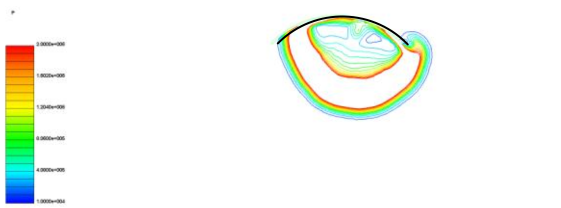

(b) 14 μsec

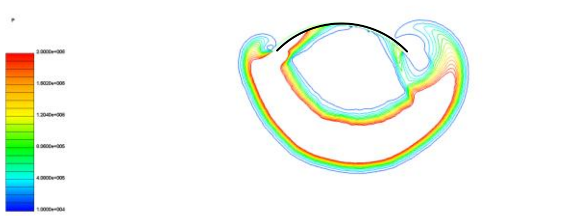

(c) 24 μsec

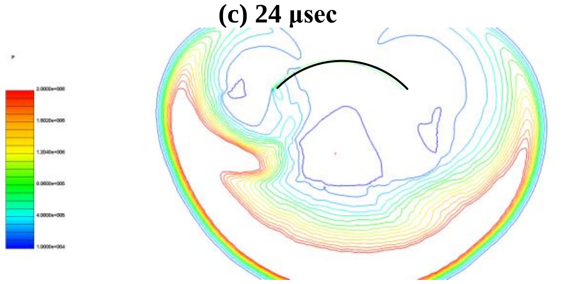

(d) 56 μsec

Figure 13 Pressure contours. *Model-2 α = 135 deg, θ =75 deg.*

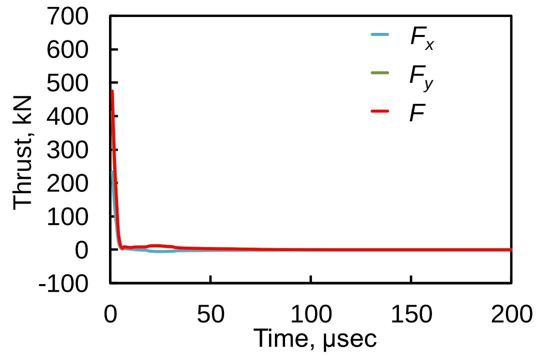

Figure 14 Thrust history. *Model-2 α = 135 deg, θ = 60 deg.*

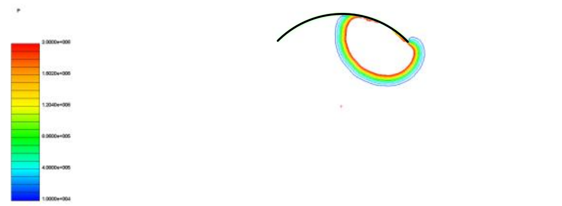

(a) 7 μsec

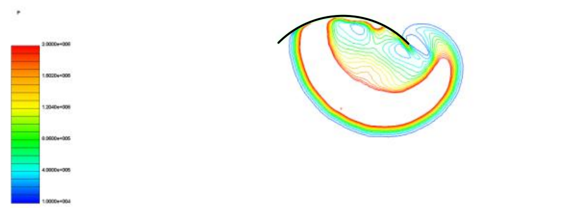

(b) 14 μsec

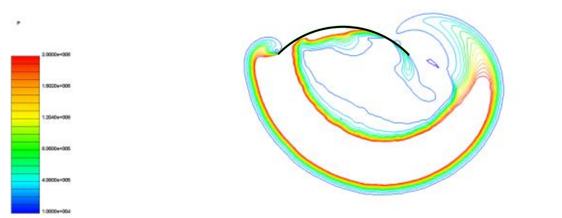

(c) 26 μsec

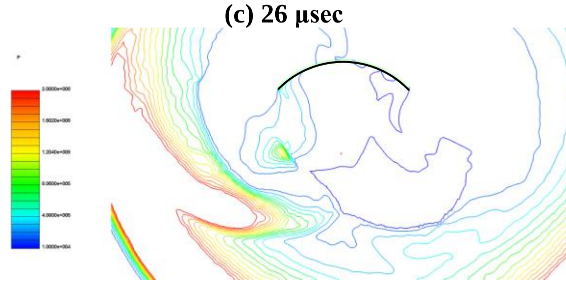

(d) 96 μsec

Figure 15 Pressure contours. *Model-2 α = 135 deg, θ=60 deg.*

x-component thrust recovers and y-component thrust decreases. At t = 96 μs, thrust becomes zero (see Fig. 15(d), t_4')

Comparing with Model-1, y-component thrusts are larger and x-component thrusts are smaller, since Model-2 has a wider shape, or a larger cone angle (α = 90 deg and 135 deg for Model-1 and 2, respectively).

From these results, it is found that the directions of impulse vectors are determined by the direction of local surface vectors of laser-irradiation spots. This is because; i) force vectors induced by the shockwaves are the products of local pressures and local surface elements, ii) total impulse reaches about 90% at initial 10 μsec, and iii) during this duration, pressure, induced by the shockwave, acting on the surface vectors are localized at near laser-irradiation spot.

C. Relationships of Impulse-bits and laser irradiation positions

From the results of thrust histories, impulse-bits were obtained through the time integration of the thrusts for various cases for Models-1 to P.

Relationships of impulse-bits and laser irradiation positions are plotted in Figs.16 (a) for Model-1, (b) Model-2 and (c) Model-P.

In both Models-1 and 2 cases, the maximum total impulse-bits are obtained at θ = 90 deg where y-component impulse-bits are also maximum and x-components being zero.

On the other hand, when irradiated at smallest θs, or near the right edges, total impulse-bits become minimum where y-component impulse-bits are also minimum and x-components being maximum.

Since a local force induced by a shock wave is a product of a local pressure and a surface element vector, the force vector has a direction of the surface vector, which is +y-direction when θ = 90 deg and mostly +x-direction when smallest θ s, or near the right edge.

On the other hand, in Model-2, y-component impulses are much larger than those of x-components. Since the Model-2 has more planar shape, smaller x-component surface vectors throughout the surface result in smaller x-component impulses.

Fig. 16(c) shows computed relationships between impulse-bit and laser spot in Model-P.

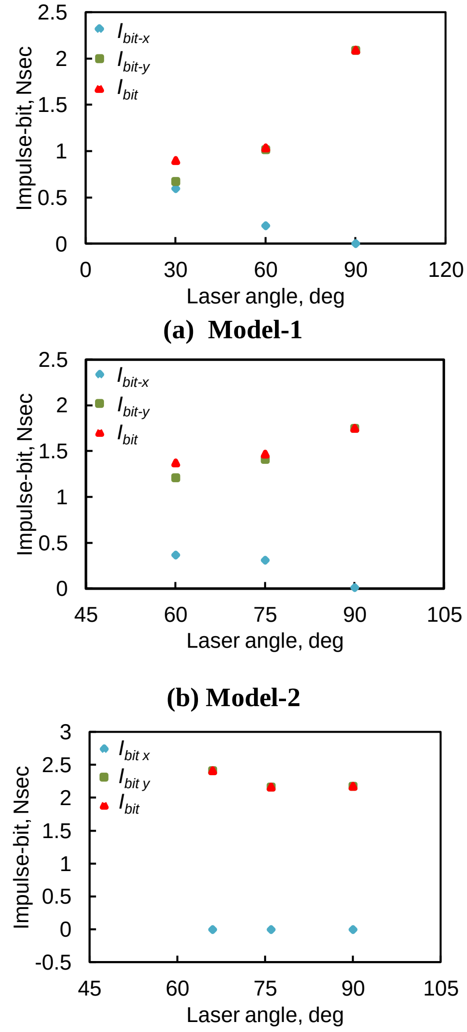

(a) Model-1

(b) Model-2

(c) Model-P

Figure 16 Relationship between Impulse-bit and laser irradiation positions.

Since there are no x-component surface vectors in Model-P due to its planar shape, a total x-component impulse is zero. There are slight differences in impulses, showing larger impulse when irradiated at the edge than the center. This is because of the longer duration of laser-induced pressure than center acting on the lower surface in this case.

Among three models, the Model-1 showed the largest impulse at θ = 90 deg.

In previous reports by Mori et al., it was shown that for laser thrusters with conical and parabolic nozzles, in which focused high-power laser pulses are irradiated at the cones, smaller cone angles of the nozzles showed higher impulse characteristics. Similar to this tendency, the Model-1 showed better thrust performances, since it has smaller cone angles.

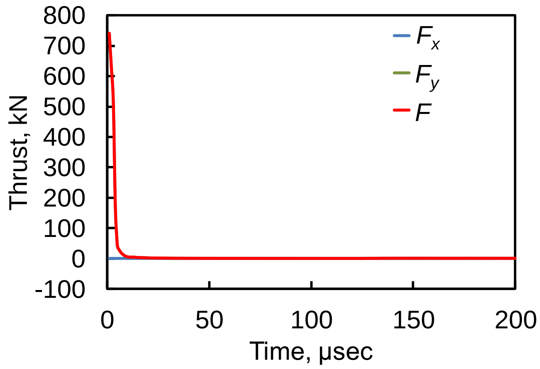

Figure 17 Thrust history. *Model-P α = 180 deg, θ = 90 deg (center).*

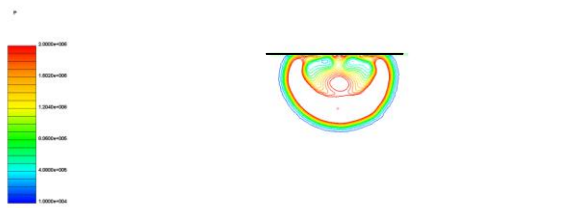

(a) 13 μsec

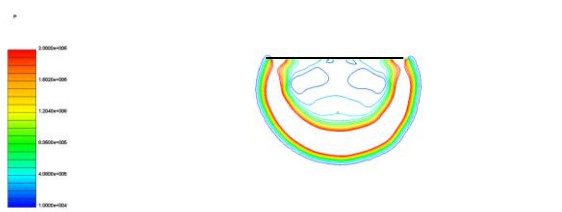

(b) 18 μsec

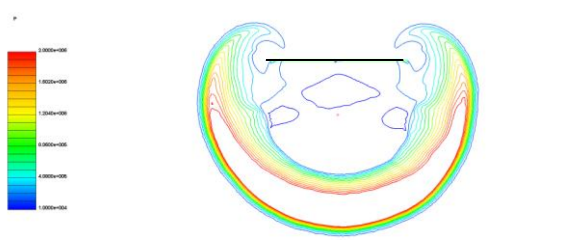

(c) 39 μsec

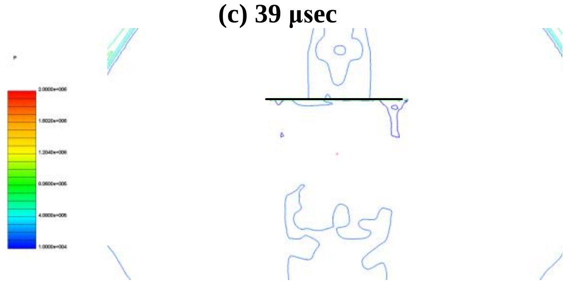

(d) 134 μsec

Figure 18 Pressure contours. Model-*P α = 180 deg, θ = 90 deg (center).*

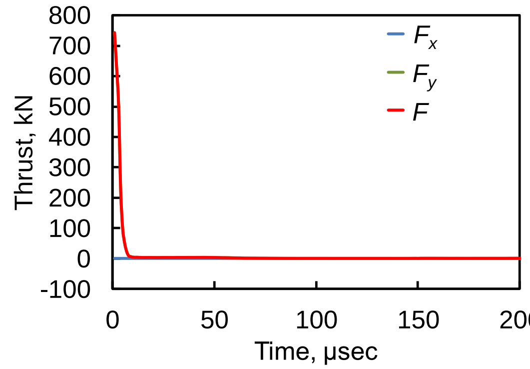

Figure 19 Thrust history. *Model-P α = 180 deg, θ = 76 deg (a spot between the center and edge).*

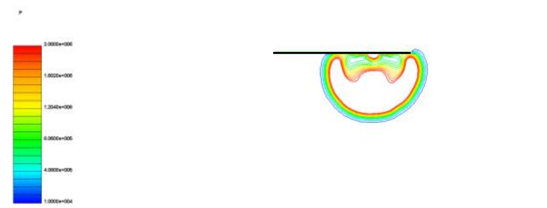

(a) 12 μsec

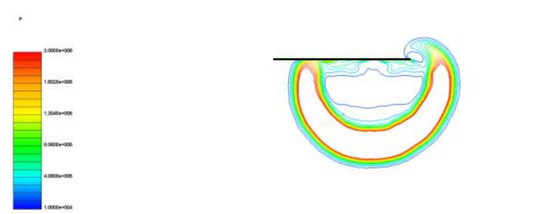

(b) 20 μsec

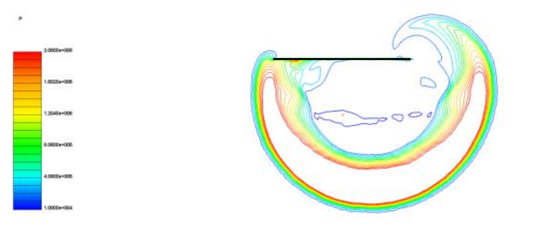

(c) 34μsec

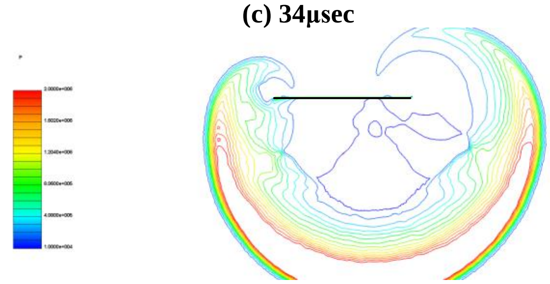

(d) 57 μsec

Figure 20 Pressure contours. *Model-P α = 180 deg, θ = 76 deg (a spot between the center and edge).*

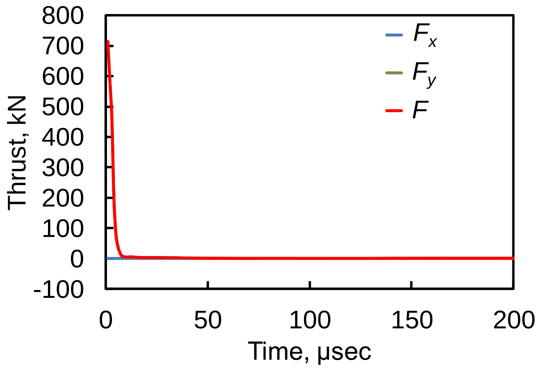

Figure 21 Thrust history. *Model-P α = 180 deg, θ = 66 deg (edge).*

(a) 7 µsec

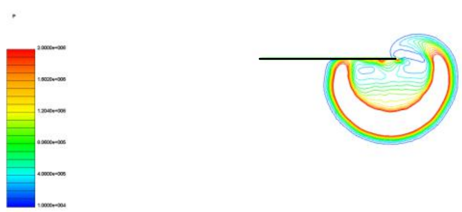

(b) 15 µsec

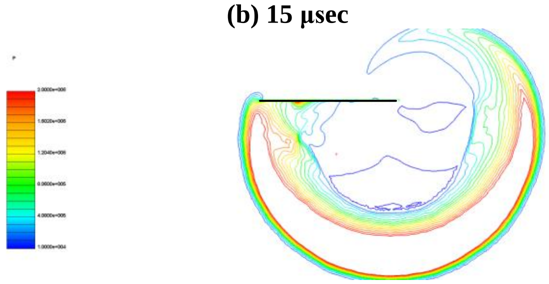

(c) 50 µsec

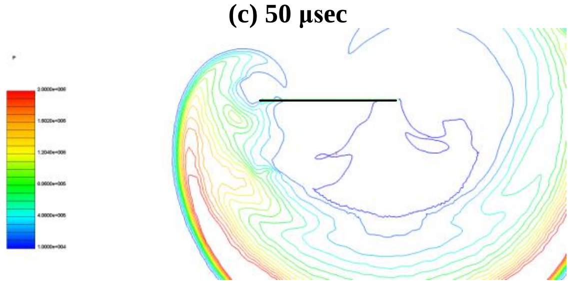

(d) 80 µsec

Figure 22 Pressure contours. *Model-P α = 180 deg, θ = 66 deg (edge).*

D. Histories of Thrust and Pressure Contours (Model-P)

Fig. 17 and 18, respectively, show the thrust history and corresponding pressure contours using Model-P for θ = 90 deg (center). In Fig. 17, for θ = 90 deg (center), an explosion starts at t = 0 µs. An initial y-component thrust is about 700 kN. After t = 13 µs, or an abrupt drop of the thrust, the variation becomes moderate (see Fig. 18(a), t_1). A shock wave front reaching a target edge at t = 18 µs (see Fig. 18(b), t_2). After t = 18 µs, y-component thrust crosses zero (see Fig. 18(c), t_3). At t = 134 µs, a total thrust converges into zero (see Fig. 18(d), t_4).

Fig. 19 and 20, respectively, show the thrust history and corresponding pressure contours using Model-1 for θ = 76 deg (a spot between the center and edge). In Fig. 19, for θ = 76 deg (a spot between the center and edge), an explosion starts at t = 0 µs. An initial y-component thrust is about 700 kN. At t = 12 µs, a shock wave reaches an edge of the target (see Fig. 20(a), t_1'). After an abrupt drop of the thrust, the variation becomes moderate at t = 20 µs (see Fig. 20(b), t_1'). A shock wave reaches another edge of the target at t = 34 µs (see Fig. 20(c), t_3'). At t = 57 µs, a thrust converges into zero (see Fig. 20(d), t_4')

Fig. 21 and 22, respectively, show the thrust history and corresponding pressure contours using Model-1 for θ = 66 deg (edge). In Fig. 21, for θ = 66 deg (edge), an explosion starts at t = 0 µs. An initial y-component thrust is about 700 kN. At t = 7 µs, a shock wave reaches an edge of the target (see Fig. 22(a), t_1'). After an abrupt drop of the thrust, the variation becomes moderate at t = 15 µs (see Fig. 22(b), t_1'). A shock wave reaches another edge of the target at t = 50 µs (see Fig. 22(c), t_3'). At t = 80 µs, a thrust converges into zero (see Fig. 22(d), t_4')

Ⅳ.Experimental setup and method

A schematic of experimental setup for impulse vector measurement is shown in Fig.23. Laser pulses from TEA-CO_2 laser (LUMONICS, TE822HP, wavelength: 10.6 µm, pulse energy: 2 J) were irradiated on a target with semicircular surface. A two-dimensional impulse vector generated with the laser ablation of the target was measured with a two-axis-pendulum thrust stand shown in Fig.24.

This thrust stand can measure both longitudinal (x-axis, parallel to laser beam) and transverse (y-axis) components of the impulse vector simultaneously. It consists of an arm hung with two-stage knife edges each of them being a pivot independently for the measurement of each component of displacement of the arm. To monitor each component of the displacement, an LED displacement sensor (OMRON, Z4W-V25R, spatial resolution: 10 µm) was used for each axis. At each measurement, calibration was performed in which an arbitrary impulse vector was applied through the perfectly inelastic collision of an aluminum ball, hung with a thin string, to the target.

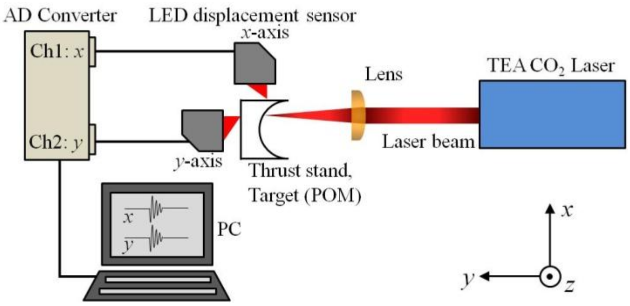

Figure 23 Experimental setup.

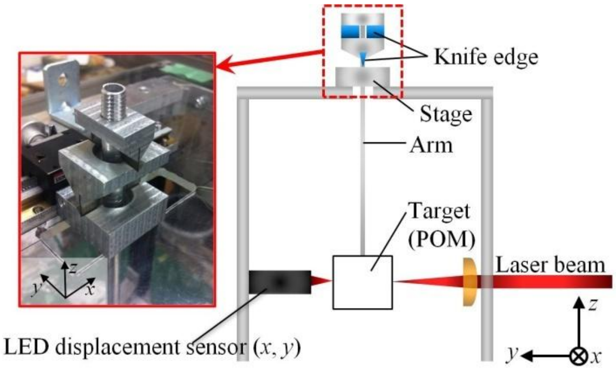

Figure 24 Schematics of thrust stand

Geometry of the target is identical to that of Model-1 employed in the numerical simulation, in which its surface consists of polyoxymethylene (POM, or polyacetal) known as the best material to obtain large impulses for pulsed CO_2 laser ablation in atmosphere. Angle of laser irradiation spot, or θ, were changed from 90deg to 15deg by changing horizontal positions of target, as shown in Fig.25. Moreover, influence of lens-target distance was also examined.

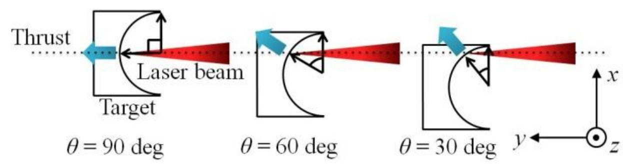

Figure 25 Variation of angle of laser irradiation spot.

V. Experimental results and discussion

Variations of *x*- and *y*- components of impulse-bit vectors with laser irradiation position are plotted in Fig.26. It can be seen that at center (θ = 90 deg) a *y*-component of impulse vector becomes largest. On the other hand, with approaching edge (or with decreasing θ) *x*-components increase and *y*- components decrease. At θ = 15 deg (near edge), an *x*-component of impulse vector becomes largest.

Comparing the results from the experiment (Fig.16) and numerical simulation, above mentioned tendencies are qualitatively similar. However, decreases of experimental results measured at near edge are more significant than those obtained in numerical simulation. This is attributed to the effect of interaction of incoming laser beam and surface of the target, which reduces effective beam energy on the target surface. Since the edge of the beam radius of the laser beam is passing near the surface of the target especially at θ = 15 deg, breakdown plasmas tend to occur along the surface far before the focal point, as shown in Fig.25, reducing effective energy at the focal point.

Effect of lens-target distance on impulse are shown in Fig.27. As own be seen, the optimum distance is at 130mm, 30% further than a focal length for various θ cases.

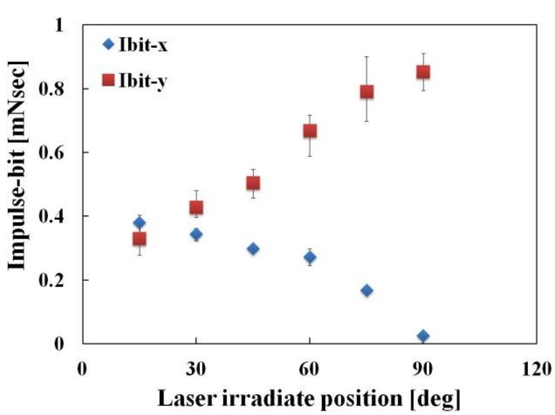

Figure 26 Relationship between Impulse-bit and laser irradiation positions

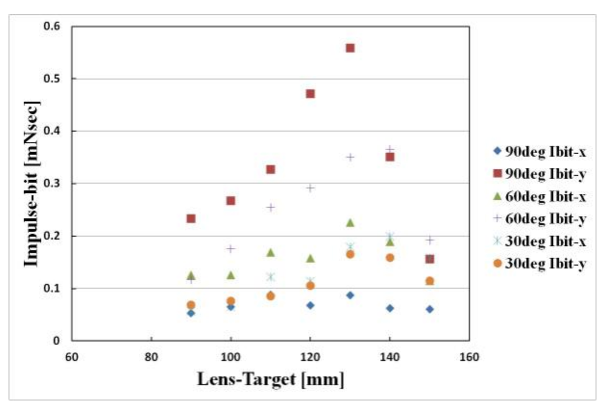

Figure 27 Relationship between Impulse-bit and lens-target distance

VI. Conclusions

A fundamental investigation was conducted on interaction of a focused high-power laser pulse, or blast wave, and the surface with arbitrary shape. Numerical simulation on characteristics of impulse, or thrust, vector generation on the surface was conducted. As the first step of the simulation, for simplicity, some fundamental shapes of the surface, or a vehicle, were assumed, which were planar and semicircular bodies, and shock-surface interactions were investigated. In addition, an experimental investigation on impulse vector characteristics was also performed.

From these results, it was shown that a composition of the impulse vector (or each component) reached about 90% of total impulse at initial 10 μsec. In addition, it was also shown that during this duration, a significantly high-pressure region, induced by the shockwave, acting on the surface vectors, which induces a primary thrust, was localized at near laser-irradiation spot. Since thrust vectors induced by the shockwaves were the products of local pressures and local surface elements, it was found that the directions of impulse vectors were primarily determined by the direction of local surface vectors of laser-irradiation spots. Effect of lens-target distance on impulse are the optimum distance is at 130mm, 30% further than a focal length for various θ cases.

References

1) Kantrowitz, A. R., “The Relevance of Space,”*Aeronautics and Astronautics*, Vol. 9, No. 3, pp. 35, 1971
2) Kantrowitz, A. R., “Propulsion to Orbit by Ground Based Lasers,” *Astronautics and Aeronautics*, Vol. 9, No. 3, pp. 40-42, 1972.
3) Pirri, A. N., and Weiss, R. F., “Laser Propulsion,” AIAA Paper 72-719, 1972.
4) Pirri, A. N., Schlier, R., and Northam, D., “Momentum Transfer and Plasma Formation Above a Surface with a High-Power CO_2 Laser,”*Applied Physics Letters*, Vol. 21, No. 3, pp. 79-81, 1972.
5) Prri, A. N., Monsler, M. J., and Nebolsine, P E., “Propulsion by Absorption of Laser Radiation,” *AIAA Jounal*, Vol. 12, No. 9, pp. 1254-1261, 1974.
6) Ageev, V. P., Barchukov, A. I., Bunkin, F. V., Konov, V. I., Korobeinikov, V. P., Putjatin, B. V., and Hudjakov, V. M., “Experimental and Theoretical Modeling of Laser Propulsion,”*ActaAstronautica*, Vol. 7, No. 1, pp. 79-90, 1980.
7) Myrabo, L. N., Libeau, M. A., Meloney, E. D., Bracken, R. L., and Knowles, T. B., “Pulsed Laser Propulsion Performance of 11-cm Parabolic ‘Bell’ Engines Within the Atmosphere,” AIAA Paper 2002-3783, May 2002.
8) Mori, K., Komurasaki, K., and Arakawa, Y., “Nozzle Scale Optimum for the Impulse Generation in a Laser Pulsejet,”*Journal of Spacecraft and Rocket*, Vol. 41, No. 5, pp. 887-889, 2004.
9) Phipps, C., Birkan, M., Bohn, W., Eckel, H. A., Horisawa, H., Lippert, T., Michaelis, M., Rezunkov, Y., Sasoh, A., Schall, W., Scharring, S., and Sinko, J., “Review: Laser-Ablation Propulsion,”*Journal of Propulsion and Power*, Vol. 26, No. 4, pp. 609-637, 2010.
10) Katsurayama, H., Komurasaki, K., Hirooka, Y., Mori, K., and Arakawa, Y., “Numerical Analyses of Exhaust and Refill Processes of a Laser Pulse Jet,”*Journal of Propulsion and Power*, Vol. 24, No. 5, pp. 999-1006, 2008.